

X-ray Absorption Fine Structure Combined with X-ray Fluorescence Spectrometry. Improvement of Spectral Resolution at the Absorption Edges of 9–29 keV

Yasuo Izumi,^{*,†} Hiroyasu Nagamori,[†] Fumitaka Kiyotaki,[†] Dilshad Masih,[†] Taketoshi Minato,[†] Eric Roisin,[‡] Jean-Pierre Candy,[‡] Hajime Tanida,[§] and Tomoya Uruga^{*,§}

Interdisciplinary Graduate School of Science and Engineering, Tokyo Institute of Technology, Nagatsuta 4259-G1-16, Midori-ku, Yokohama 226-8502, Japan, Laboratoire de Chimie Organometallique de Surface, UMR CNRS–CPE 9986, France, and Japan Synchrotron Radiation Research Institute, Kohto 1-1-1, Mikazuki-cho, Sayo 679-5198, Japan

X-ray absorption near-edge structure (XANES) suffers from core–hole lifetime broadening at a higher energy absorption edge, such as Sn K (29 keV, $\Gamma_K = 8.49$ eV). To overcome this problem, emitted Sn $K\alpha_1$ fluorescence from sample was counted using high-energy-resolution fluorescence spectrometer in the XANES measurements. Experimental energy resolution (5.0 eV) was consistent with theoretical values based on the Rowland configuration of the spectrometer. The absorption edge became steeper compared to conventional spectra. The white-line peak due to Sn^{II} species became remarkably sharper and more intense in the Sn $K\alpha_1$ -detecting Sn K-edge XANES for Pt–Sn/SiO₂. To support the semiclassical theory of resonant Raman scattering for the explanation of observed elimination of lifetime width, more resolved XANES data at Cu K, Pb L₃, and Sn K in this work were convoluted (filtered) with a Lorentzian of each core–hole lifetime width. The processed data resembled generally well corresponding XANES spectrum measured in transmission mode. The verification based on *ab initio* XANES calculations was also performed.

X-ray absorption near-edge structure (XANES) is the fluctuation of X-ray absorption intensity in the range of ~100 eV including the absorption edge. It has been widely applied to analysis and speciation for surface,¹ macromolecules,¹ life science,² environmental science,³ and catalysis.^{2,4} Among various spectroscopic methods, XANES is advantageous to sensitively monitor the chemical state of an X-ray absorbing element. In addition, it often

reflects the site symmetry and the type of coordinated atom(s) for an X-ray absorbing element.^{1,2} Geometric information deduced from XANES is complementary to bonding distance and the coordination number extracted from extended X-ray absorption fine structure (EXAFS) that ranges ~1000 eV beyond the absorption edge.

The chemical state and the site symmetry are primarily reflected within ± 10 eV range from the absorption edge as preedge peak(s), absorption-edge energy shift, and “white-line” peak above the absorption edge.^{1,2} In principle, all the XANES spectra are affected by the core–hole lifetime broadening. This broadening is especially serious at higher energy absorption edge due to the increase of core–hole lifetime width (Γ).^{5,6}

The elimination of lifetime broadening was first reported for the Dy L₃-edge XANES by using a secondary high-energy-resolution ($\Delta E = 0.3$ eV) fluorescence spectrometer in combination with synchrotron wiggler beamline.⁷ The resolved preedge peaks due to 2p → 4f transition and sharper, more intense white-line peak were observed for Dy metal, oxide, and nitride when the Dy $L\alpha_1$ fluorescence was detected with energy bandwidth smaller than Γ_{L3} (4.17 eV; Table 1).⁸ More resolved Pt L₃ ($\Gamma_K = 5.31$ eV) and Cu K-edge ($\Gamma_K = 1.55$ eV) spectra were also reported by the detection of Pt $L\alpha_1$ ⁹ and Cu $K\alpha_1$,¹⁰ respectively.

We have developed and applied this XAFS technique combined with X-ray fluorescence (XRF) spectrometry at V,^{11–13} Cr,¹⁰ Cu,^{10,14,15} and As K-edges¹⁶ and Pb L₃-edge.^{17,18} The Γ values for Cu K, Dy L₃, Pt L₃, Pb L₃, and Sn K increase starting from 1.55 to

- (5) Nishihata, Y.; Emura, S.; Maeda, H.; Kubozono, Y.; Harada, M.; Uruga, T.; Tanida, H.; Yoneda, Y.; Mizuki, J.; Emoto, T. *J. Synchrotron Radiat.* **1999**, *6*, 149–151.
- (6) Nishihata, Y.; Kamishima, O.; Kubozono, Y.; Maeda, H.; Emura, S. *J. Synchrotron Radiat.* **1998**, *5*, 1007–1009.
- (7) Hämäläinen, K.; Siddons, D. P.; Hastings, J. B.; Berman, L. E. *Phys. Rev. Lett.* **1991**, *67*, 2850–2853.
- (8) Krause, M. O.; Oliver, J. H. *J. Phys. Chem. Ref. Data* **1979**, *8*, 329–338.
- (9) de Groot, F. W. F. *Top. Catal.* **2000**, *10*, 179–186.
- (10) Izumi, Y.; Nagamori, H. *Bull. Chem. Soc. Jpn.* **2000**, *73*, 1581–1587.
- (11) Izumi, Y.; Kiyotaki, F.; Yagi, N.; Vlaicu, A.; Nisawa, A.; Fukushima, S.; Yoshitake, H.; Iwasawa, Y. *J. Phys. Chem. B* **2005**, *109*, 14884–14891.
- (12) Izumi, Y.; Kiyotaki, F.; Yoshitake, H.; Aika, K.; Sugihara, T.; Tatsumi, T.; Tanizawa, Y.; Shido, T.; Iwasawa, Y. *Chem. Lett.* **2002**, 1154–1155.
- (13) Izumi, Y.; Kiyotaki, F.; Yoshitake, H.; Aika, K.; Sugihara, T.; Tatsumi, T.; Tanizawa, Y.; Shido, T.; Iwasawa, Y. *Chem. Commun.* **2002**, 2402–2403.

* To whom correspondence should be addressed. E-mail: yizumi@chemenv.titech.ac.jp; urugat@spring8.or.jp.

[†] Tokyo Institute of Technology.

[‡] CNRS.

[§] Japan Synchrotron Radiation Research Institute.

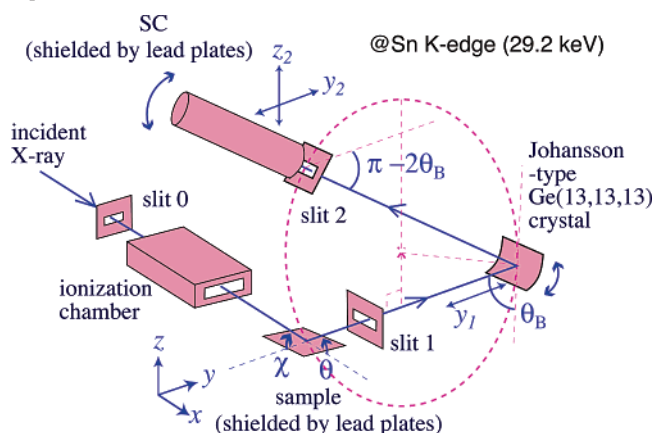
- (1) Stöhr, J. *NEXAFS Spectroscopy*; Springer: Berlin-Heidelberg, 1992.
- (2) Koningsberger, D. C.; Prins, R., Eds. *X-ray Absorption—Principles, Applications, Techniques of EXAFS, SEXAFS, and XANES*; John Wiley & Sons: New York, 1988.
- (3) Van Grieken, R. E.; Markowicz, A. A., Eds. *Handbook of X-ray Spectrometry*, 2nd ed.; Marcel Dekker: New York, 2002.
- (4) Iwasawa, Y., Ed. *X-ray Absorption Fine Structure for Catalysts and Surfaces*; World Scientific: Singapore, 1996.

Table 1. Energy Values for Absorption Edges and Emission Peaks, Lifetime Widths for the Core Hole and Emission Peaks, and Energy Resolution of Fluorescence-detecting XAFS

absorption edge		E (eV) ^a	$\Gamma_{\text{K or L}_3}$ (eV) ⁸	emission detected	E (eV) ^a	Γ (eV) ⁸	ΔE (eV) ^b	refs
V	K	5463.9	1.01	K α_1	4952.2	1.26	2.0	11–13
Cr		5988.8	1.08	K $\beta_{1,3}$	5946.7	~1.08	2.0	10, 15
Mn		6537.6	1.16	K $\beta_{1,3}$	6490.5	~1.16	0.8	29
Fe		7111.2	1.25	K $\beta_{1,3}$	7058.0	~1.25	1.6	30
Cu		8980.3	1.55	K α_1	8047.8	2.01	1.1	this work, 10, 14
As		11865	2.14	K α_1	10543.7	3.08	1.3	16
Sn		29194.7	8.49	K α_1	25271.3	11.24	5.0	this work
Dy	L ₃	7789.7	4.17	L α_1	6495.2	5.6	0.8	7
Pt		11562	5.31		9442.3			9
Pb		13040.6	5.81		10551.5		5.0	this work, 17, 18

^a Energy values for metal.²⁰ ^b Energy resolution including the contribution of beamline.

Scheme 1. Schematic View of Our Fluorescence Spectrometer Combined with XAFS Beamline



8.49 eV (Table 1). This work reports experimental trials to overcome the problem of core-hole lifetime broadening at the Sn K-edge. The feasibility of this technique at the edge is demonstrated. The improvement of spectral resolution was found to be more significant at higher energy edges utilizing this technique.

Further, the XANES data obtained combining with XRF were convoluted (filtered) with a Lorentzian and compared to XANES data obtained in transmission mode at the edges of 9–29 keV (Cu K, Pb L₃, and Sn K). The $\Delta E/E$ (E , photon energy) for the beam incident on the sample was $\sim 10^{-4}$. The ΔE of our fluorescence spectrometer was theoretically estimated to 1.1, 1.9, and 4.0 eV at Cu K-, Pb L₃-, and Sn K-edges, respectively, including the contribution of beamline.¹⁴ Comparable values were experimentally achieved when the vertical openings of slits 1 and 2 equipped in the spectrometer (Scheme 1) were set to 0.5, 2.0, and 2.0 mm, respectively.

METHODS

Samples. Standard samples CuCl₂ (>95%, Wako), 2PbCO₃·Pb(OH)₂ (first grade, Wako), Sn metal (>99.5%, Wako), SnO

(>99.9%, Wako), and SnO₂ (>99.9%, Aldrich) were used as received. The samples were diluted to metal (X-ray absorbing element) 1.5–5.0 wt % by thorough mixing with boron nitride (special grade, Wako).

The Pt–Sn/SiO₂ catalyst was prepared by the following procedure.¹⁹ The slurry of Pt(NH₃)₄(OH)₂ (Strem) was reacted with the surface hydroxyl groups of silica (specific surface area 200 m² g⁻¹, Degussa) for 10 h. After filtration, the obtained powder was calcined in flowing O₂ + N₂ (1:4) and then reduced in flowing H₂ at 673 K (Pt/SiO₂). Sn(*n*-C₄H₉)₄ was introduced to the reduced Pt/SiO₂ powder in the presence of H₂ (3.0 kPa) and reacted at 373 K. The Pt–Sn/SiO₂ sample was treated under flowing H₂ at 673 K before it was introduced and sealed in a glass cell. Since the X-ray data were acquired a few weeks later than the cell was sealed, the possibility of contamination by air of the sample could not be excluded. The Pt loading was 2.5 wt % as metal and the atomic ratio Sn/Pt was 1.0.

Operating Conditions of Synchrotron Ring, Beamline, and the Fluorescence Spectrometer. The X-ray measurements were performed at the undulator beamline BL10XU at SPring-8, Japan. The storage ring energy was 8.0 GeV, and the ring current was 100–71 mA. A Si(111) double-crystal monochromator was used. A rhodium-coated double mirror was inserted in the incident X-ray beam path in order to suppress higher harmonics except for the Sn K-edge study. The X-ray fluorescence from the sample was analyzed by a homemade Rowland-type spectrometer equipped with a Johansson-type Ge crystal (Saint-Gobain) and a NaI(Tl) scintillation counter (SC; Oken).

The arrangement of the spectrometer is depicted in Scheme 1. The Rowland radius was set to 220 mm and the higher-order reflections of Ge(111) were used. The size of slit 0 in front of I₀ ionization chamber was fixed to 1.0 × 1.0 mm². The sample was set in a plane tilted from a horizontal plane toward the direction of the incident X-ray by an angle θ and also toward the direction perpendicular to incident X-ray in the same horizontal plane by an angle χ . The values θ and χ were set to 6–13 and 7–13 deg, respectively. The horizontal opening of receiving slit 1 (100 mm apart from the center of sample) and of slit 2 in front of SC was fixed at 8.0 mm. The vertical opening of the two slits was varied between 0.5 and 7.5 and between 0.5 and 2.0 mm, respectively, as the compromise between ΔE and photon counts.^{10,15}

(19) Humblot, F.; Didillon, D.; Lepeltier, F.; Candy, J. P.; Corker, J.; Clause, O.; Bayard, F.; Basset, J. M. *J. Am. Chem. Soc.* **1998**, *120*, 137–146.

All the X-ray measurements were performed at 290 K. Maximum incident photon flux at the BL10XU was $\sim 10^{13}$ s $^{-1}$. Throughout the XANES spectrum measurements, the undulator gap and the parallelism of the monochromator crystals were optimized to maximize the X-ray beam flux at each data point. The average I_i counts at SC were 2×10^2 s $^{-1}$ for copper(II) chloride (Cu K-edge), 6×10^3 s $^{-1}$ for 2PbCO $_3$ ·Pb(OH) $_2$ (Pb L $_3$ -edge), and 3×10 s $^{-1}$ for Pt–Sn/SiO $_2$ (Sn K-edge). The energy values of monochromator and fluorescence spectrometer were reproduced within ± 0.1 and ± 0.2 eV, respectively.

X-ray Emission and Absorption Spectrum Measurements.

The Cu K α_1 emission spectra were measured for copper(0) metal and copper(II) chloride with the excitation energy set at 9000.1 eV. The Ge(444) reflection was used. The emission energy for Cu metal was calibrated to 8047.8 eV 20 (Bragg angle $\theta_B = 70.630$ deg). The fluorescence spectrometer was tuned to the Cu K α_1 peak top and Cu K-edge XANES spectrum was measured. The scan step of monochromator was ~ 0.28 and ~ 0.56 eV in the energy range 8957–9021 and 9021–9063 eV, respectively. The dwell time of each data point was 10–15 s.

The Pb L α_1 emission spectra were measured for Pb 0 metal and 2Pb II CO $_3$ ·Pb II (OH) $_2$ with the excitation energy set at 13064.3 eV. The Ge(555) reflection was used. The emission energy for Pb metal was calibrated to 10551.5 eV 20 ($\theta_B = 64.083$ deg). The fluorescence spectrometer was tuned to the Pb L α_1 peak top, and Pb L $_3$ -edge XANES spectrum was measured. The scan step of monochromator was ~ 0.30 and ~ 0.60 eV in the energy range 13 016–13 077 and 13 077–13 125 eV, respectively. The dwell time of each data point was 40 s.

The Sn K α_1 emission spectra were measured for Sn 0 metal and Pt–Sn/SiO $_2$ catalyst with the excitation energy set at 29 235.0 eV. The Pt–Sn/SiO $_2$ catalyst was sealed in Pyrex glass cell equipped with a Kapton film window of 12.5- μ m thickness. The cell was purged with 81 kPa of hydrogen and placed in a sample holder. The Ge(13,13,13) reflection was used. The emission energy for Sn metal was calibrated to 25 271.3 eV 20 ($\theta_B = 77.527$ deg). The fluorescence spectrometer was tuned to the Sn K α_1 peak top, and Sn K-edge XANES spectrum was measured. The scan step of monochromator was ~ 0.45 and ~ 1.9 eV in the energy range 29 137–29 227 and 29 227–29 303 eV, respectively. The dwell time of each data point was 20–100 s. All the absorption edge energy values were calibrated to each reference value (Table 1). 20

The signal/background ratio was $> 1.2 \times 10^2$ for copper(II) chloride (Cu K-edge), $> 1.7 \times 10^2$ for 2PbCO $_3$ ·Pb(OH) $_2$ (Pb L $_3$ -edge), and > 1.8 for Pt–Sn/SiO $_2$ (Sn K-edge). To suppress the detection of scattered X-rays (via air and parts of spectrometer), sample and SC were thoroughly covered with lead plates of 1–5-mm thickness except for the incident beam entrance, the exit of X-ray fluorescence from sample, and the entrance of X-ray fluorescence reflected via Ge crystal (Scheme 1) in the Pb L $_3$ - and Sn K-edges study.

Analysis. Background subtraction of the raw XANES spectrum was performed using a Victoreen parameter. A smooth spline function was calculated in the postedge region, and the spectrum was normalized at $k \approx 4$ Å $^{-1}$ from the edge (derivative maximum). In a procedure similar to data smoothing, normalized XANES data

were convoluted using Lorentzian. 21

$$I_i(\text{convoluted}) = I_i(\text{data}) + \sum_{j=1}^N \{I_j(\text{Lorentzian}) \times I_j(\text{neighboring data}) \times \text{energy interval}_j(\text{eV}) \times \text{weighting constant}\} \quad (1)$$

The convolution using a Gaussian or pseudo-Voigt function was also performed. As these operations were performed for normalized data and thus the summation in eq 1 included more preedge zero intensity data as the data i above the absorption edge approached nearer the edge, the convoluted XANES spectrum came to be tilted slightly upward as a function of energy. Therefore, the background subtraction was performed again from the convoluted spectrum. Thus obtained data was renormalized.

The effect of experimental energy resolution was also verified by ab initio calculations. 13 A code FEFF version 8.1 22 was applied to generate theoretical XANES spectra in self-consistent field and multiple scattering calculation modes. The energy shift of pure imaginary “optical” potential was varied to evaluate the elimination of the lifetime broadening effect.

RESULTS

Cu K-Edge. The full width at a half-maximum (fwhm) of the Cu K α_1 emission peak was 2.3 eV measured for CuCl $_2$. 14 The natural width of Cu K α_1 is 2.01 eV. 8 Under the condition that the convolution of ΔE (1.1 eV) is smaller than the Γ_K value for copper (1.55 eV), Cu K α_1 -detecting Cu K-edge XANES spectrum was measured for CuCl $_2$ (Figure 1a). The more resolved peaks at 8989 and 8979.5 eV $^{23-27}$ are justified by convolution in the Analysis section compared to conventional XANES (Figure 1b).

Pb L $_3$ -Edge. The fwhm of the Pb L α_1 emission peak was 8.8 eV measured for 2PbCO $_3$ ·Pb(OH) $_2$. The lifetime width of Pb L $_3$ is 5.81 eV. 8 The width of $_{82}\text{Pb}$ M $_5$ may be similar to that for $_{66}\text{Dy}$ (1.4 eV). 7 Thus, the ΔE of the fluorescence spectrometer was estimated to 5.0 eV including the contribution of beamline. This value is worse than theoretical estimation 28 (1.9 eV). The major reason of this discrepancy is that the vertical opening of receiving slit 1 (Scheme 1) was set to as much as 7.5 mm to know the lower detection limit of Pb contained in a sample under a fixed condition of the fluorescence spectrometer. 17,18

Under the condition that the ΔE is smaller than the Γ_{L_3} value for lead (5.81 eV), Pb L α_1 -detecting Pb L $_3$ -edge XANES spectrum

- (21) In eq 1, the Lorentzian was centered at the energy of each data point i . The maximum intensity of Lorentzian was one. The width of Lorentzian was varied around the Γ value for the absorption edge. The weighting constant was optimized for each edge to better fit the processed data to the conventional experimental XANES data (1.0, 0.15, and 1.0 for Cu K-, Pb L $_3$ - and Sn K-edges, respectively).
- (22) Ankudinov, A. L.; Ravel, B.; Rehr, J. J.; Conradson, S. D. *Phys. Rev. B* **1998**, *58*, 7565–7576.
- (23) Kau, L.; Spira-Solomon, D. J.; Penner-Hahn, J. E.; Hodgson, K. O.; Solomon, E. I. *J. Am. Chem. Soc.* **1987**, *109*, 6433–6442.
- (24) Pickering, I. J.; George, G. N. *Inorg. Chem.* **1995**, *34*, 3142–3152.
- (25) Shadle, S. E.; Penner-Hahn, J. E.; Schugar, H. J.; Hedman, B.; Hodgson, K. O.; Solomon, E. I. *J. Am. Chem. Soc.* **1993**, *115*, 767–776.
- (26) Kuroda, Y.; Yoshikawa, Y.; Konno, S.; Hamano, H.; Maeda, H. *J. Phys. Chem.* **1995**, *99*, 10621–10628.
- (27) Saini, N.; Lanzara, A.; Bianconi, A.; Oyanagi, H. *Phys. Rev. B* **1998**, *58*, 11768–11773.
- (28) Georgopoulos, P.; Knapp, G. S. *J. Appl. Crystallogr.* **1981**, *14*, 3–7.

(20) Bearden, J. A. *Rev. Mod. Phys.* **1967**, *39*, 78–124.

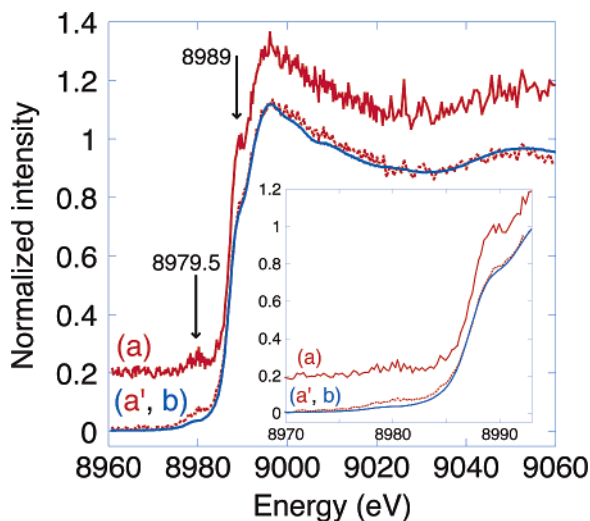


Figure 1. Normalized Cu K-edge XANES spectrum for CuCl_2 measured by detecting $\text{Cu K}\alpha_1$ fluorescence (a) or in transmission mode (b). The data a were convoluted by a Lorentzian of core-hole lifetime width for Cu K level (1.55 eV) to be a' (dotted line). (Inset) Magnified preedge and absorption edge region.

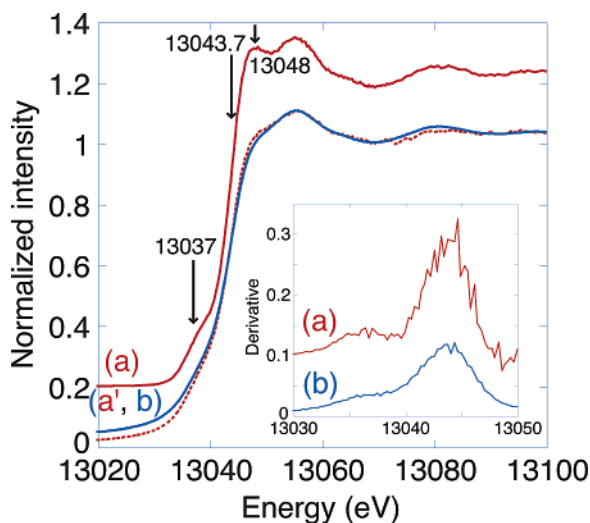


Figure 2. Normalized Pb L_3 -edge XANES spectrum for $2\text{PbCO}_3 \cdot \text{Pb(OH)}_2$ measured by detecting $\text{Pb L}\alpha_1$ fluorescence (a) or in transmission mode (b). The data a were convoluted by a Lorentzian of core-hole lifetime width for Pb L_3 level (5.81 eV) to be a' (dotted line). (Inset) First-derivative spectra of normalized XANES (a, b).

was measured for $2\text{PbCO}_3 \cdot \text{Pb(OH)}_2$ (Figure 2a). The more resolved peaks at 13 048 and 13 037 eV are justified by convolution in the Analysis section compared to conventional XANES (b). The resolution improvements are clearly demonstrated in their first-derivative spectra (Figure 2, inset). Essentially, the absorption edge became far steeper with this method.

Sn K-Edge. The fwhm of the Sn $\text{K}\alpha_1$ emission peak was 12.3 eV for Sn metal (Figure 3, dots). The natural width of Sn $\text{K}\alpha_1$ line is 11.24 eV.⁸ The ΔE of the fluorescence spectrometer was estimated to 5.0 eV including the contribution of beamline. This value is essentially consistent with theoretical estimation²⁸ (4.0 eV).

Under the condition that the ΔE is smaller than the Γ_K value for tin (8.49 eV), Sn $\text{K}\alpha_1$ -detecting Sn K-edge XANES spectra were measured for Sn metal and Pt–Sn/SiO₂. In the spectrum for Sn

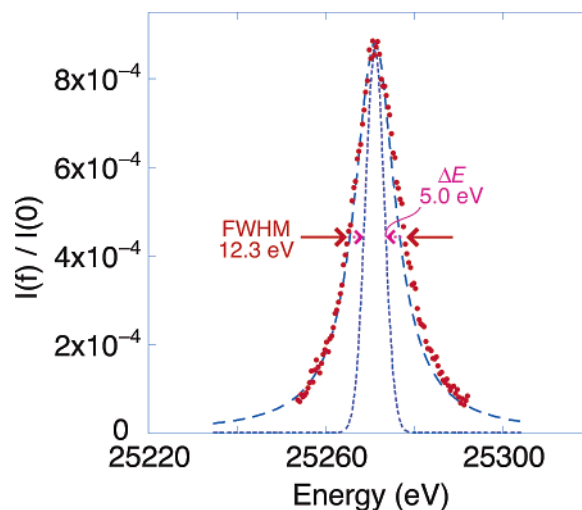


Figure 3. Sn $\text{K}\alpha_1$ emission spectrum for Sn metal. Each data point is presented as a dot. Broader and narrower dotted lines are the Sn $\text{K}\alpha_1$ lifetime width (11.24 eV) and the energy resolution of fluorescence spectrometer (5.0 eV) including the contribution of beamline.

metal (Figure 4A(a)), the first intense peak at 29 201.7 eV became sharper and more intense compared to that measured in the transmission mode (Figure 4A(b)). The absorption edge became steeper by selective detection of Sn $\text{K}\alpha_1$ based on the first-derivative data (Figure 4A, inset). For the Sn K-edge data of Pt–Sn/SiO₂, the improvement of spectral resolution was remarkably pronounced for the white-line peak at 29 206.3 eV (Figure 4B-(a)). The absorption edge became also steeper at 29 200.3 eV (Figure 4B, inset).

ANALYSIS

Cu K-Edge. The Cu $\text{K}\alpha_1$ -detecting XANES data in Figure 1a was convoluted using Lorentzian, Gaussian, or both. Lorentzian convolution nicely transformed the data to the one similar to conventional data if adequate Lorentzian width was chosen. When Gaussian was used, the spectrum did not change substantially from original data because the feet of the Gaussian peak rapidly diminish to the bottom and thus the effective number of data points for convolution with Gaussian in eq 1 were very limited compared to the convolution using Lorentzian. When the pseudo-Voigt function was used, data were transformed essentially due to the Lorentzian portion only. Thus, the fwhm value for Lorentzian was systematically varied around 1.55 eV.

The convoluted spectrum using a Lorentzian of 1.55-eV width was depicted in Figure 1a'. The processed data were essentially identical with conventional spectrum b except for the minor difference in the pre-edge region 8975–8985 eV (vide supra for the reason).

Pb L3-Edge. The fwhm value of the Lorentzian was varied around 5.81 eV. The Pb $\text{L}\alpha_1$ -detecting XANES was effectively transformed into data similar to a conventional spectrum when convoluted with a Lorentzian of 5.81-eV width (Figure 2a'). The processed data were nearly identical with conventional spectrum b except for a minor difference in the region below 13 040 eV.

Sn K-Edge. When the fwhm value of the Lorentzian varied for Sn $\text{K}\alpha_1$ -detecting XANES measured for Pt–Sn/SiO₂, the white-line peak became less intense and broader as the Lorentzian width progressively grew from 5.00 to 11.24 eV. The processed data

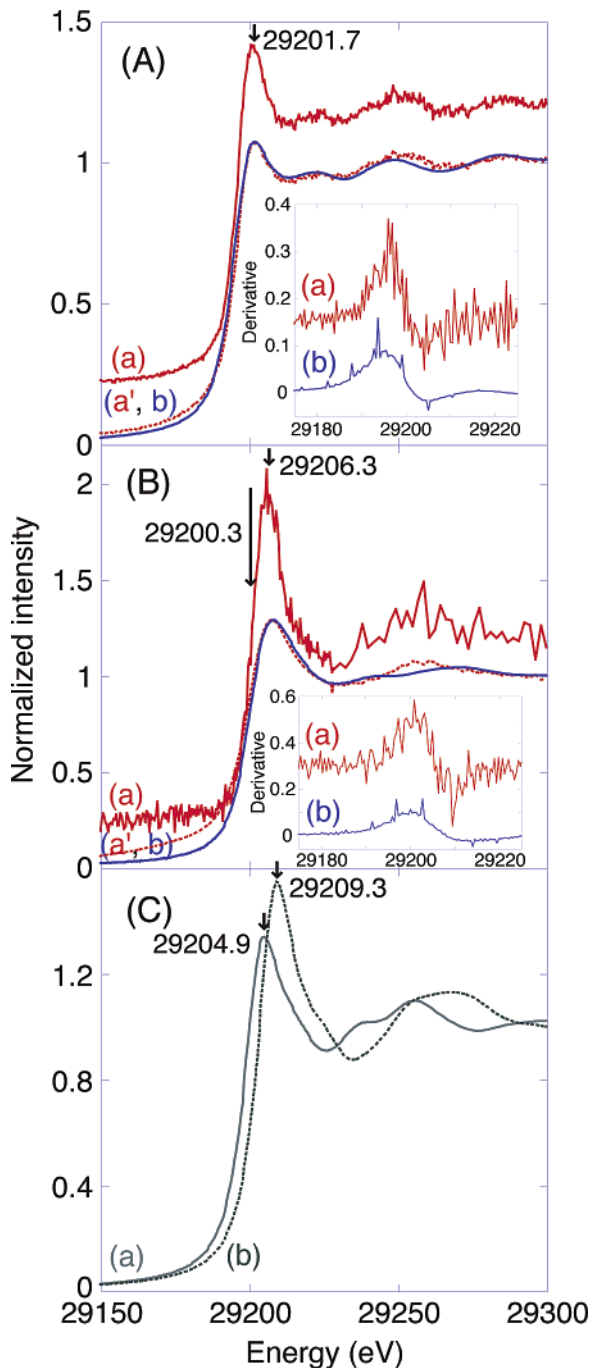


Figure 4. Normalized Sn K-edge XANES spectra for Sn metal (A) and Pt–Sn/SiO₂ catalyst (2.5 wt % Pt; Sn/Pt atomic ratio, 1.0) (B) measured by detecting Sn K α_1 fluorescence (a) or in transmission mode (b). The data a were convoluted by a Lorentzian of core–hole lifetime width for Sn K level (8.49 eV) to be a' (dotted line). (Inset) First-derivative spectra of normalized XANES (a, b). (C) Sn K-edge XANES for Sn^{II}O (a) and Sn^{IV}O₂ (b) measured in transmission mode.

when the fwhm value was 8.49 eV [Figure 4A(a') and 4B(a')] resembled most corresponding conventional spectra A(b) (Sn metal) and B(b) (Pt–Sn/SiO₂), respectively, except for the differences in the region below 29190 eV for both samples and the postedge region between 29 245 and 29 260 eV for Pt–Sn/SiO₂.

In summary, convolution of XANES data combined with XRF nicely reproduced conventional XANES obtained in transmission

mode using a Lorentzian. However, the coincidence was not complete in the case of Sn K-edge data for Pt–Sn/SiO₂.

DISCUSSION

Reason for the Improvement of XANES Profile Resolution. The improvement of spectral resolution was pronounced in the region of ± 10 eV from the absorption edges of Cu K, Pb L₃, and Sn K by detecting Cu K α_1 , Pb L α_1 , and Sn K α_1 , respectively, with smaller ΔE (1.1, 5.0, and 5.0 eV, respectively) than their core–hole lifetime width (1.55, 5.81, and 8.49 eV, respectively). The XANES method combined with XRF was found to be advantageous at higher energy absorption edges because the increase of lifetime width is greater than the increase of instrumental ΔE (Table 1). At the lower energy K-edges of V,^{11–13} Cr,^{10,15} and Mn,²⁹ the ΔE only due to beamline was similar/larger than each Γ_K value (Table 1).

The steepness of the absorption edge was significantly improved for Pb L₃- and Sn K-edges (Figures 2 and 4) in selective fluorescence detection mode compared to transmission mode. The improvement was directly visualized as their first-derivative data (derivative peak sharpness and intensity) in Figures 2 (inset) and 4A and B (inset), respectively.

The theoretical basis of enhanced resolution observed in Figures 1, 2, and 4 was formulated in the Appendix section.^{7,30} The X-ray fluorescence is considered associated with dipole transition from shell B to A, e.g., from L₃ to K (K α_1) or from M₅ to L₃ (L α_1). Based on eq A1, when the energy resolution to monitor the fluorescence, $B(\omega_2)$, is smaller than Γ_A , Lorentzian lifetime broadening will be suppressed by $B(\omega_2)$, and sharper features near the absorption edge can be observed.

This theoretical prediction was in accord with the data in this work (Figures 1, 2, and 4) using a high- ΔE Rowland-type spectrometer to satisfy the condition $B(\omega_2) < \Gamma_A$. To confirm this effect, the Cu K α_1 -, Pb L α_1 -, and Sn K α_1 -detecting XANES data were convoluted using a Lorentzian with each core–hole lifetime width. All the processed data resembled fairly well corresponding XANES spectra measured in transmission mode except for a minor discrepancy of Sn K-edge data for Pt–Sn/SiO₂. In summary, these data convolution tests supported the theoretical rationale of resolution improvement for XANES in the condition $B(\omega_2) < \Gamma_A$.

This effect was also confirmed based on the energy shift of pure imaginary “optical” potential in ab initio calculations. A similar spectrum was calculated to conventional XANES (Figure 4A(b)) when the shift was set to zero (Figure 5c) whereas the profile of Sn K α_1 -detecting XANES measured in the condition $B(\omega_2) < \Gamma_A$ was well reproduced when the shift was set to -2.0 eV (Figure 5a, b).

Feasible Applications of Fluorescence-Selecting XANES Satisfying the Condition $B(\omega_2) < \Gamma_A$. (1) Cu K-Edge.

The weak preedge peak at ~ 8979 eV has been reported for Cu^{II} compounds due to 1s \rightarrow 3d transition.^{23–27} The shoulder peak on the absorption edge between 8986 and 8988 eV was also reported for Cu^{II}(2,5-dithiahexane)₂(ClO₄)₂, [creatinium]₂⁺[Cu^{II}Cl₄]²⁻, and Cu^{II}(imidazole)₄(ClO₄)₂, but no shoulder peak was found for Cu^{II}SO₄·5H₂O.²³ The peak was assigned to shakedown transition. The 1s \rightarrow 4p transition (the final state (1s)¹...(3d)⁹(4p)¹) and ligand-to-

(29) Grush, M. M.; Christou, G.; Hämäläinen, K.; Cramer, S. P. *J. Am. Chem. Soc.* **1995**, *117*, 5895–5896.

(30) Glatzel, P.; Bergmann, U. *Coord. Chem. Rev.* **2005**, *249*, 65–95.

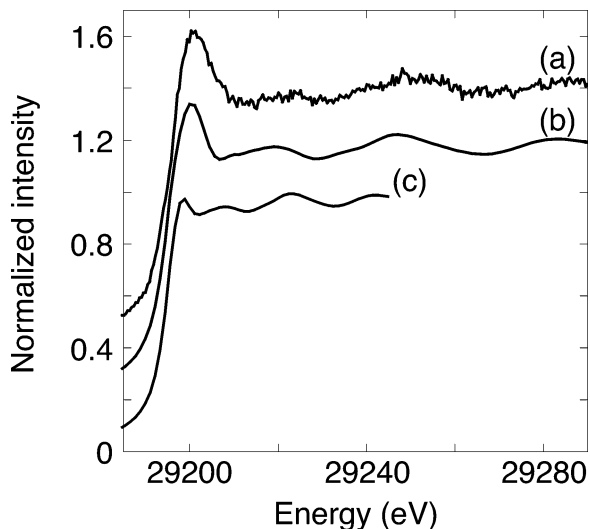


Figure 5. Normalized Sn K-edge XANES spectrum for Sn metal measured by detecting Sn $K\alpha_1$ fluorescence (a) and corresponding Sn K-edge XANES generated by FEFF in SCF and FMS modes (b, c). The energy shift to pure imaginary “optical” potential was set to -2.0 (b) and 0 eV (c). The edge energy for spectra b and c was corrected to spectrum a.

metal charge transfer (LMCT) take place at the same time. In total, the final state is $(1s)^1 \cdots (3d)^{10} \underline{L}(4p)^1$, where \underline{L} means ligand hole.^{23–25}

Polarized XAFS studies were performed to discuss the Cu site symmetry utilizing the anisotropy of $1s \rightarrow 3d$ and $1s \rightarrow 4p$ peak intensity for $Cu^{II}Cl_2$ ²⁴ and $Bi_2Sr_2CaCu_2O_{8+\delta}$ single crystals.²⁷ Utilizing the improvement of spectral resolution depicted in Figure 1a, type of ligand atom and site symmetry will be discussed into more detail also for powder samples.

(2) *Pb L_3 -Edge.* Due to the difference between Γ_K for copper and Γ_{L_3} for lead (Table 1), conventional Pb L_3 absorption edge (Figure 2b) was apparently broader than that of Cu K-edge (Figure 1b). Pb $L\alpha_1$ -detecting Pb L_3 -edge XANES spectrum was measured satisfying the condition $B(\omega_2) < \Gamma_{L_3}$. Due to the effect to make steeper the absorption edge, two shoulder peaks at the foot ($13\text{--}037$ eV) and the end ($13\text{--}048$ eV) of the absorption edge came to be resolved (Figure 2a).

The presence/absence of the peak at $13\text{--}048$ eV was reported to judge the speciation of Pb^{II} .^{31–33} The shoulder peak was observed for coordinatively saturated Pb^{II} sites (e.g., $2PbCO_3 \cdot Pb(OH)_2$) but not for unsaturated Pb^{II} species (e.g., ion-exchanged Pb^{2+} on the surface). The resolved Pb $L\alpha_1$ -detecting Pb L_3 -edge data were reported for the more accurate speciation in the application of environmental chemistry.^{17,18}

(3) *Sn K-Edge.* Due to the difference of Γ_{L_3} for lead and Γ_K for tin (Table 1), conventional Sn K-edge data were even broader (Figure 4b). Sn $K\alpha_1$ -detecting Sn K-edge XANES spectrum was measured, satisfying the condition $B(\omega_2) < \Gamma_{L_3}$ for Sn metal (Figure 4A(a)) and Pt–Sn/SiO₂ (Figure 4B(a)). The intense peak energy above the edge for Pt–Sn/SiO₂ (29206.3 eV) corresponded

to the Sn^{II} state compared to values for standard Sn^0 (Figure 4A), Sn^{II} , and Sn^{IV} (Figure 4C). The postedge pattern of Figure 4B(a) was similar to that for $Sn^{II}O$ (Figure 4C(a)). Thus, the major Sn species in Pt–Sn/SiO₂ was concluded to be Sn^{II} .³⁴

In a comparison between Figure 4A(a) and B(a), the intense peak above the edge was more pronounced for the Sn^{II} species. The convoluted spectrum with a Lorentzian did not completely reproduce corresponding conventional data only in the case of Sn K-edge for Pt–Sn/SiO₂ (Figure 4B(a')) among all spectra processed in this paper. The reason is unclear, but the resonant excitation effect may be enhanced for the electronic transition to bound/semibound state, such as the π^* state and empty state of Cu 3d. A minor discrepancy was also detected in the preedge region between convoluted and conventional Cu K-edge (Figure 1a', b). This effect was proposed for the increase of $1s \rightarrow 3d$ pre-edge peak intensity in the Fe $K\beta_{1,3}$ -detecting Fe K-edge for $Fe^{II/III}$ species.³⁵ The contribution of resonance excitation effect for specific peaks near the edge is not included in eq 1 for convolution.

In a reverse point of view to utilize this data discrepancy for Sn, valence-selective peak enhancement may be enabled and applied to Sn K-edge studies for such as heterogeneous catalysts,³⁶ gas sensor,³⁷ and environmental samples,^{38,39} where lifetime broadening has hampered quantitative analysis.

CONCLUSIONS

X-ray fluorescence-detecting XAFS method was successfully applied to the Sn K-edge in combination with a highly brilliant, low-emittance synchrotron beam. At higher energy absorption edges, the effect to detect the X-ray fluorescence with an energy bandwidth smaller than each core–hole lifetime width was more remarkable to obtain steeper absorption edge. Preedge peak, peak on the absorption edge, and white-line peak hidden in the broadened absorption edge in conventional spectra became revealed. The improvement of energy resolution by this method was supported by the data convolution with a Lorentzian of each core–hole lifetime width and also by ab initio XANES calculations (energy shift of pure imaginary “optical” potential). As applications of this method, improved speciation of low concentrations of Pb^{2+} was enabled to determine the surface reaction mechanism of Pb^{2+} .^{17,18} Selective detection of enhanced Sn^{II} or Sn^{IV} white-line peak will enable more quantitative characterization of redox catalysis sites and oxidic Sn sites for supported Pt–Sn catalysts. In situ population ratio change of coexisting Sn^0 , Sn^{II} , and Sn^{IV} species for Pt–Sn catalysts was suggested based on ^{119}Sn Mössbauer measurements.⁴⁰

(34) The Sn–O bonds at 2.06 \AA (the coordination number $N = 3\text{--}4$) based on the curve fit analysis of Sn K-edge EXAFS supported this conclusion. Sn–Pt shell was also given at a bond distance 2.70 \AA with the N of $8\text{--}10$. Once formed Pt–Sn alloy on SiO₂ surface may be partially oxidized.

(35) Heijboer, W. M.; Glatzel, P.; Sawant, K. R.; Lobo, R. F.; Bergmann, U.; Barrea, R. A.; Konongsberger, D. C.; Weckhuysen, B. M.; de Groot, F. M. F. *J. Phys. Chem. B* **2004**, *108*, 10002–10011.

(36) Onda, A.; Komatsu, T.; Yashima, T. *J. Catal.* **2004**, *221*, 378–385.

(37) Grandjean, D.; Benfield, R. E.; Nayral, C.; Maisonnat, A.; Chaudret, B. *J. Phys. Chem. B* **2004**, *108*, 8876–8887.

(38) Sakakibara, N.; Takahashi, Y.; Yamaguchi, Y.; Shibata, K.; Uruga, T. *Chem. Lett.* **2004**, *33*, 264–265.

(39) Takahashi, Y.; Sakakibara, N.; Nomura, M. *Anal. Chem.* **2004**, *76*, 4307–4314.

(40) Stievano, L.; Wagner, F. E.; Calogero, S.; Recchia, S.; Dossi, C.; Psaro, R. *Stud. Sur. Sci. Catal.* **2000**, *130D*, 3903–3908 (Corma, A., Melo, F. V., Mendioroz, S., Fierro, J. L. G., Eds.).

(31) Rouff, A. A.; Elzinga, E. J.; Reeder, R. J. *Environ. Sci. Technol.* **2004**, *38*, 1700–1707.

(32) Huang, F.; Jao, H.; Hung, W.; Chen, K.; Wang, C. *J. Phys. Chem. B* **2004**, *108*, 20458–20464.

(33) Rose, J.; Moulin, I.; Hazemann, J.; Masion, A.; Bertsch, P. M.; Bottero, J.; Mosnier, F.; Haehnel, C. *Langmuir* **2000**, *16*, 9900–9906.

ACKNOWLEDGMENT

The experiments were performed under the approval of the SPring-8 Program Review Committee, 2004A0122-NX-np and 2003B0386-NXa-np at the Sn K-edge, 2001B0004-CX-np and 2001A0022-NX-np at the Pb L₃-edge, and 1999B0220-NX-np and 1998A0295-NX-np at the Cu K-edge. Y.I. is thankful for financial support from the Grant-in-Aid for Scientific Research (B13555230), Encouragement of Young Scientists (B14740401, A12740376), and Exploratory Research (08874066) from the Ministry of Education, Culture, Sports, Science, and Technology, Toray Science Foundation (98-3901), and Yamada Science Foundation (2000). This paper is part 16 in the series.

APPENDIX

X-ray fluorescence is considered associated with dipole transition from shell B to A. When incident photon energy $\hbar\omega_1$ is enough above the absorption edge, the fwhm of the fluorescence is $\Gamma_A + \Gamma_B$. When $\hbar\omega_1$ is set in the vicinity of the absorption edge, the cross section $\sigma(\omega_1)$ for the fluorescence is formulated

based on semiclassical interpretation of resonant Raman scattering,^{7,30}

$$\sigma(\omega_1) \propto \int_0^\infty d(\hbar\omega_2) \int_0^\infty d\epsilon B$$
$$(\omega_2) \frac{\omega_2}{\omega_1} \frac{E_B - E_A + \hbar\omega_1 - \hbar\omega_2}{E_B - E_A} \frac{\Gamma_A}{(\hbar\omega_1 + E_A - \epsilon)^2 + \Gamma_A^2/4}$$
$$\frac{\Gamma_B}{(\hbar\omega_1 + E_B - \hbar\omega_2 - \epsilon)^2 + \Gamma_B^2/4} \sigma_A (\epsilon - E_A) \quad (\text{A1})$$

where $\hbar\omega_1$ is scattered photon energy, ϵ is the kinetic energy of photoelectron, E_B and E_A are the B and A shell binding energies, and σ_A is the total A-shell photoabsorption cross section.

Received for review July 13, 2005. Accepted August 24, 2005.

AC0512453